

# Mechanochemical effects for some Al<sub>2</sub>O<sub>3</sub> powders of dry grinding

T. BAN, K. OKADA, T. HAYASHI\*, N. ŌTSUKA

*Department of Inorganic Materials, Tokyo Institute of Technology, O-okayama, Meguro, Tokyo 152, Japan*

Three kinds of Al<sub>2</sub>O<sub>3</sub> powders, i.e. two kinds of low-soda Al<sub>2</sub>O<sub>3</sub> with average particle sizes of 3.9 and 0.6 μm and an electrofused Al<sub>2</sub>O<sub>3</sub> with an average particle size of 21.8 μm, were ground for up to 300 h in a dry vibration ball mill. Variations in particle-size distribution, specific surface area, crystallite size, lattice strain, effective temperature factor and lattice constant were examined against milling time. The mechanism of grinding was found to differ between low-soda Al<sub>2</sub>O<sub>3</sub> and electrofused Al<sub>2</sub>O<sub>3</sub>. The mechanochemical effects on these Al<sub>2</sub>O<sub>3</sub> powders occurred in the order decrease of crystallite size → increase of effective temperature factor → increase of lattice strain. The length of the *a*-axis was clearly increased by a prolonged grinding. The difference in the ground state of three specimens was attributed to differences in the physical state of particles originating from the preparation methods, and also to particle size.

## 1. Introduction

Al<sub>2</sub>O<sub>3</sub> powders have been widely used in the ceramics industry, and various kinds of powders: 1. sintered Al<sub>2</sub>O<sub>3</sub>; 2. low-soda Al<sub>2</sub>O<sub>3</sub>; 3. fused Al<sub>2</sub>O<sub>3</sub>; and 4. high-purity Al<sub>2</sub>O<sub>3</sub>, may be prepared by different methods [1]. Among these, the starting raw material for categories 1 and 3 is Al<sub>2</sub>O<sub>3</sub> powder produced by the Bayer process. High-purity Al<sub>2</sub>O<sub>3</sub> is prepared by various methods and has common properties such as a small (submicrometre) particle size and purity higher than 4N grade. On the other hand, the particle size of Al<sub>2</sub>O<sub>3</sub> powders belonging to categories 1–3 is usually coarser than that of category 4. Therefore the grinding of these powders is considered to be one of the important essential processing steps.

It is well known that grinding treatment not only causes breakdown of particles but also has mechanochemical effects. The former factor corresponds to variations in particle size distribution and specific surface area. The latter appears as variation of crystallite size, lattice strain and effective temperature factor [2], which represents the degree of fluctuation of the atomic positions. Some work on the relation between grinding treatment and sinterability of Al<sub>2</sub>O<sub>3</sub> powders has been reported [3–6]. Excess grinding causes a heavy agglomeration of the powders and also an increase in weight loss of the powders, and therefore was not suitable for sintering except for initial stage, which was enhanced by the activated surface diffusion. On the other hand, examination of the mechanochemical effects for Al<sub>2</sub>O<sub>3</sub> powders has not yet been sufficiently elucidated.

Three kinds of Al<sub>2</sub>O<sub>3</sub> powders, i.e. two kinds of low-soda Al<sub>2</sub>O<sub>3</sub> with different particle sizes and an electro-

fused Al<sub>2</sub>O<sub>3</sub> were ground in a dry vibration ball mill. Variations in particle size, specific surface area, crystallite size, lattice strain, effective temperature factor and lattice constant were measured against milling time. From these data, the mechanisms of grinding and mechanochemical effects on the powders were investigated in relation to preparation methods.

## 2. Experimental procedure

The starting materials used for this study were two kinds of low-soda Al<sub>2</sub>O<sub>3</sub> with an average particle size of 0.6 μm (LS23) and 3.9 μm (LS21), both of which are produced by Nippon Light Metal Co. Ltd, Shimidzu, Japan, and an electrofused Al<sub>2</sub>O<sub>3</sub> with an average particle size of 21.8 μm (WA600) produced by Showa Denko Co. Ltd, Shiojiri, Japan. They reported chemical compositions are Al<sub>2</sub>O<sub>3</sub> 99.8, Na<sub>2</sub>O 0.02–0.06, SiO<sub>2</sub> 0.02–0.04 and Fe<sub>2</sub>O<sub>3</sub> 0.03 wt % for the low-soda Al<sub>2</sub>O<sub>3</sub>; and Al<sub>2</sub>O<sub>3</sub> 99.6, Na<sub>2</sub>O 0.2, SiO<sub>2</sub> 0.02 and Fe<sub>2</sub>O<sub>3</sub> 0.03 wt % for the electrofused Al<sub>2</sub>O<sub>3</sub>. Powder X-ray diffraction (XRD) revealed that the electrofused Al<sub>2</sub>O<sub>3</sub> contained a small amount of β-Al<sub>2</sub>O<sub>3</sub> besides α-Al<sub>2</sub>O<sub>3</sub>. Specimens LS23, LS21 and WA600 are designated S<sub>0.6</sub>, S<sub>3.9</sub> and S<sub>22</sub>, respectively. To remove the influence of various pretreatments, powders were annealed at 800 °C for 2 h before the experiments. Dry vibration milling (MB-1, Chuoh Kakohki Co. Ltd) was performed up to 300 h with a vibration number of 1000 r.p.m. The Al<sub>2</sub>O<sub>3</sub> powder of 700 g was charged in a 2-l Al<sub>2</sub>O<sub>3</sub> pot with 2 kg of Al<sub>2</sub>O<sub>3</sub> balls (20 mm in diameter) as grinding media. No atmosphere control was used in the milling experiments. After a certain milling time, 15 g of the sample was collected from the

\* Present address: Nishi-Tokyo Science University, Uenohara, Kitatsuru, Yamanashi, Japan.

pot and 1–4 g of grinding aid ( $\text{Ti}(\text{OC}_4\text{H}_9)_4$ ) was added each time to avoid agglomeration of the specimens [7] during milling. The accumulated amount of the  $\text{TiO}_2$  component in the final powders was calculated to be 0.7 wt %.

Particle-size distribution was measured by a Microtrack instrument (Nikkisoh Co. Ltd) dispersing the powders ultrasonically in a HCl solution adjusted to pH 2. Specific surface area was measured by the BET method using a nitrogen gas with a Sorptomatic 1800 instrument (Carlo Elba Co. Ltd). Size and shape of particles were observed by SEM (MSM-9, Akashi Seisakusho Co. Ltd).

XRD measurement (Geigerflex, Rigaku Co. Ltd) was made with a step scanning and fixed-time method using graphite monochromated  $\text{CuK}\alpha$  radiation. The experimental conditions were as follows: a slit system of  $1-1^\circ-0.15-0.8$  mm, a step width of  $0.004^\circ$ , and a fixed time of 4 s. Peak position, peak intensity and integral width of twelve reflections from  $20$  to  $140^\circ$  in  $2\theta$  were precisely measured and used for the calculation of lattice constant, effective temperature factor, crystallite size and lattice strain, respectively. Since the reflections of higher angles were heavily diffused and weakened by milling in specimen  $S_{0.6}$ , only six reflections could be used for the various calculations. The standards for correction of instrumental broadening of reflections and that of reflection angles were the specimen  $S_{22}$  annealed at  $1600^\circ\text{C}$  for 2 h and the Si powder (640a, NBS), respectively. Crystallite size ( $D_c$ ) and lattice strain ( $\eta$ ) were calculated by Hall's method [8] using the following formula:

$$\beta \cos \theta / \lambda = 1/D_c + 2\eta \sin \theta / \lambda \quad (1)$$

where  $\beta$  is a real integral width of specimen after corrected for instrumental broadening, and  $\lambda$  is the X-ray wavelength. Effective temperature factor ( $B_{\text{eff}}$ ) was calculated by the following formula [2]:

$$\ln(I_{\text{obs}}/I_{\text{std}}) = \ln k - 2B_{\text{eff}}(\sin^2 \theta / \lambda^2) \quad (2)$$

where  $I_{\text{obs}}$  and  $I_{\text{std}}$  were the observed intensity of the specimen and that of the standard, and  $k$  is a constant. Lattice constants of  $\alpha\text{-Al}_2\text{O}_3$  were calculated by the least-squares method using the RSLC-3 program [9].

### 3. Results

#### 3.1. Particle size and specific surface area

Fig. 1 shows SEM photographs of as-received specimens. Particles of specimen  $S_{22}$  were an irregular and angular shape. Most of the particles of specimen  $S_{3.9}$  were thick hexagonal plates. Particles of  $S_{0.6}$  were small and rounded.

Fig. 2 shows variations of specific surface area for three specimens against milling time. The increase of specific surface area of  $S_{22}$  was much higher than those of specimens  $S_{0.6}$  and  $S_{3.9}$ . This difference must correspond to the difference in grinding mechanism. It was also apparent in the difference in curve shapes that the curves of  $S_{0.6}$  and  $S_{22}$  were convex, but that of  $S_{3.9}$  was concave.

Fig. 3 shows the variation in average particle size ( $d_{50}$ ), a spherically corresponding particle size estim-

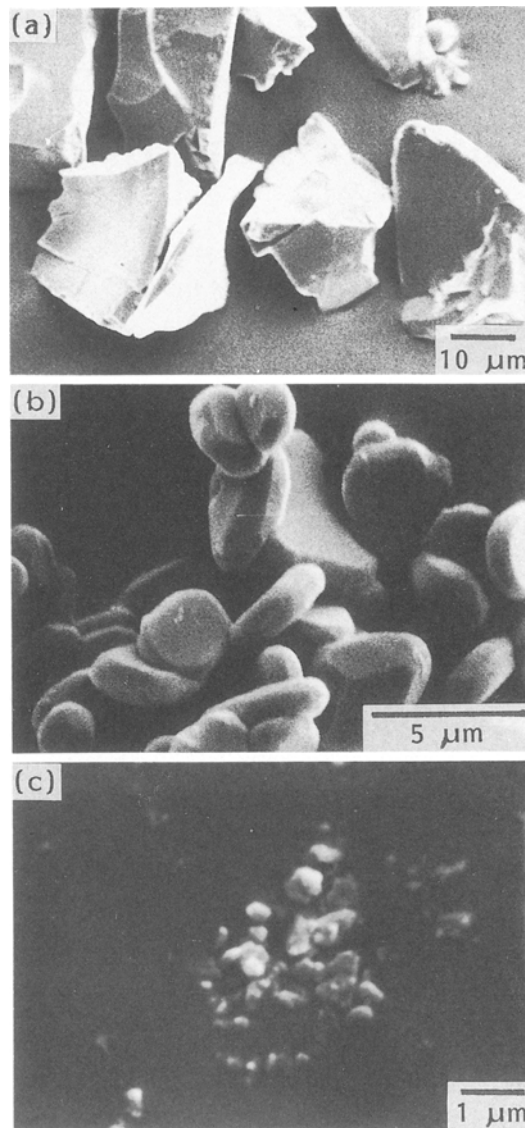


Figure 1 SEM photographs of as-received specimens. (a)  $S_{22}$ ; (b)  $S_{3.9}$ ; (c)  $S_{0.6}$ .

ated from the specific surface area ( $d_s$ ), and a crystallite size ( $D_c$ ) for three specimens against milling time. The  $d_{50}$  of the three specimens decreased with milling time:  $23.8 \rightarrow 3.4 \mu\text{m}$  in  $S_{22}$ ,  $5.2 \rightarrow 3.5 \mu\text{m}$  in  $S_{3.9}$ , and  $1.35 \rightarrow 0.97 \mu\text{m}$  in  $S_{0.6}$ . (Here, since specimens  $S_{3.9}$  and  $S_{0.6}$  after annealing were heavily agglomerated by the annealing treatment, the  $d_{50}$  data after 20 h milling were used for the initial data.) Variation of the  $d_{50}$  in  $S_{0.6}$  and  $S_{3.9}$  was apparently smaller than that in  $S_{22}$ . The  $d_{50}$  of specimen  $S_{0.6}$  decreased a little up to 180 h milling time, but was almost constant with further milling time. Variations in  $d_s$  showed a similar trend to those of  $d_{50}$ . The  $d_s$  curves of  $S_{0.6}$  and  $S_{22}$  showed a concave shape and it was considered to be the tendency for saturation. That of specimen  $S_{3.9}$ , however, showed a constant decrease up to 300 h milling.

#### 3.2. Mechanochemical parameters

Variation of crystallite size for three specimens against milling time is shown in Fig. 3. Crystallite sizes of as-annealed specimens  $S_{3.9}$  and  $S_{22}$  were very large and

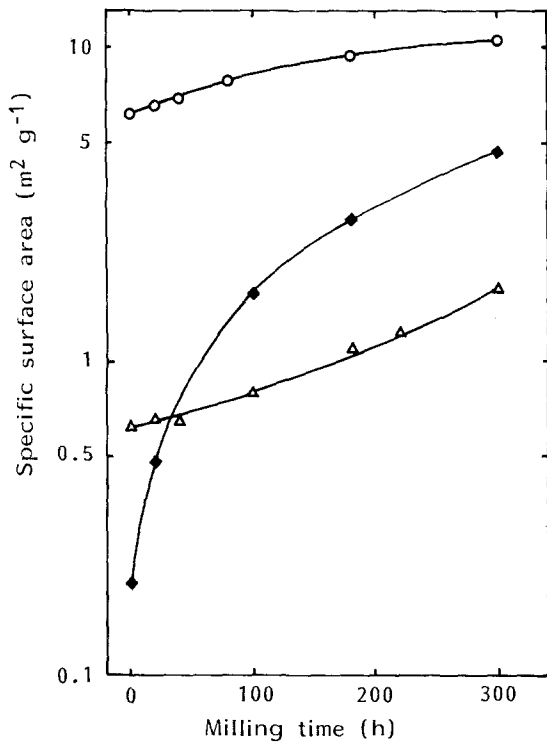


Figure 2 Variation of specific surface area against milling time for each specimen.  $\circ$ ,  $S_{0.6}$ ;  $\triangle$ ,  $S_{3.9}$ ;  $\blacklozenge$ ,  $S_{22}$ .

were taken as infinite size by this method. They decreased very rapidly as soon as the milling started and decreased to 100 nm in  $S_{3.9}$  and 88 nm in  $S_{22}$  after 300 h milling. On the other hand, the crystallite size of  $S_{0.6}$  was evidently smaller than those of the other two specimens even after annealing; it decreased further from 140 to 77 nm with 100 h milling, and kept a constant value even with further milling.

Fig. 4 shows variation in lattice strain for three specimens against milling time. The lattice strains of three as-annealed specimens showed a little difference, and that of  $S_{22}$  was the largest. Thermal stress due to the very high temperature process for the preparation of this specimen was considered to be the reason. The lattice strain was almost constant during the initial milling period up to 40 h because mechanochemical energy was almost expended by the rapid decrease in crystallite size in this period. After this period, the lattice strain began to increase with milling time. The increase in lattice strain in  $S_{3.9}$  was the smallest, but maintained a constant increasing rate even after 300 h milling. The other two specimens showed a convex curve and the increase in lattice strain in  $S_{22}$  seemed to be almost saturated by this milling time.

Fig. 5 shows variation in the effective temperature factor for three specimens against milling time. The effective temperature factors increased with the milling time, but their rates were not a constant against milling time. An increasing rate between around 50 and 100 h was especially high. The effective temperature factors of  $S_{22}$  and  $S_{0.6}$  became almost similar values after 300 h milling, and seemed to be almost saturated. That of  $S_{3.9}$  was, however, only about half of those of the other specimens, but seemed to continue to increase linearly even after 300 h milling.

Fig. 6 shows the variation of the lattice constant of  $\alpha\text{-Al}_2\text{O}_3$  against milling time. The longer the milling time, the length of the  $a$ -axis showed a more significant increase up to 220 h milling, while no change or a small decrease was observed for the length of the  $c$ -axis. Here the  $a$ -axis is parallel to the layer of the hcp structure, and the  $c$ -axis is perpendicular to it.

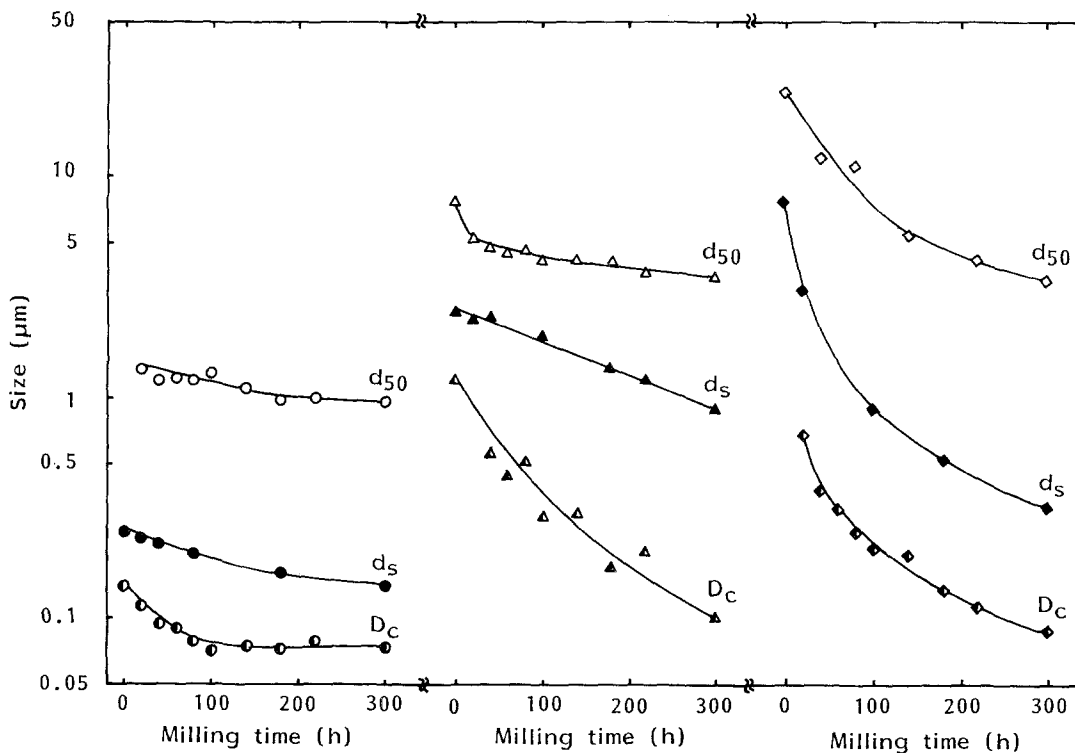


Figure 3 Variation of average particle size ( $d_{50}$ ), spherically corresponding particle size estimated from specific surface area ( $d_s$ ), and crystallite size ( $D_c$ ) against milling time for each specimen. Circles,  $S_{0.6}$ ; triangles,  $S_{3.9}$ ; diamonds,  $S_{22}$ .

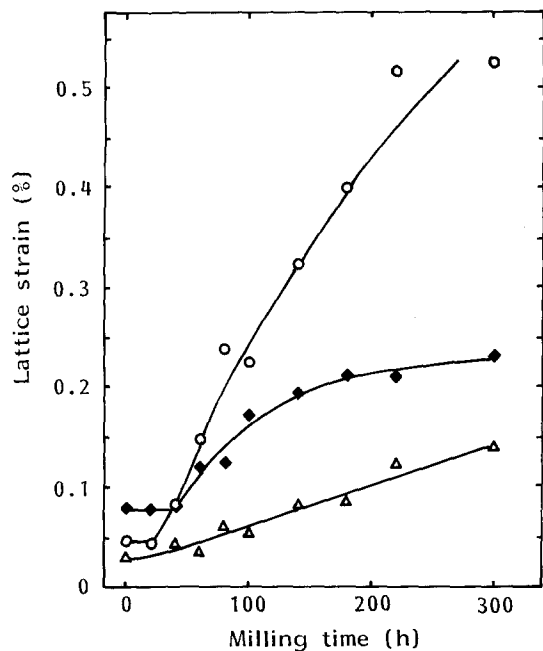


Figure 4 Variation of lattice strain ( $\eta$ ) against milling time for each specimen.  $\circ$ ,  $S_{0.6}$ ;  $\triangle$ ,  $S_{3.9}$ ;  $\blacklozenge$ ,  $S_{22}$ .

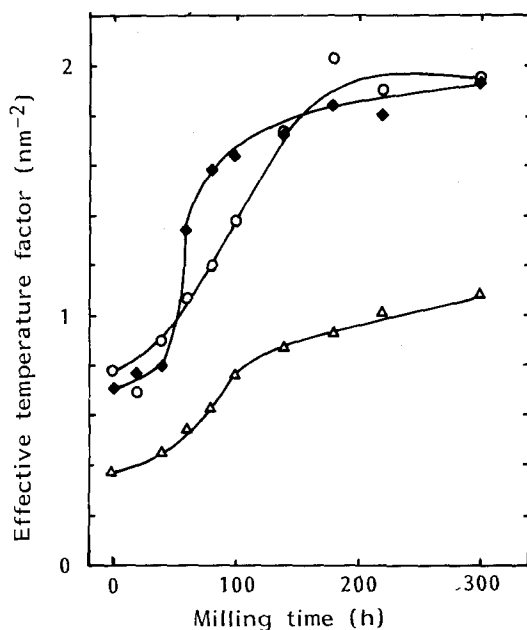


Figure 5 Variation of effective temperature factor ( $B_{\text{eff}}$ ) against milling time for each specimen.  $\circ$ ,  $S_{0.6}$ ;  $\triangle$ ,  $S_{3.9}$ ;  $\blacklozenge$ ,  $S_{22}$ .

Since the values of  $a$  and  $c$  axes for as-annealed specimens were in a good agreement with those reported for  $\alpha\text{-Al}_2\text{O}_3$  [10], variations in lattice length, especially in the  $a$ -axis, were considered to be uniform lattice deformation caused by the grinding. It was not certain what kind of structural change corresponded to this lattice deformation. Considering that the deformation in the  $a$ -axis was much larger than that in the  $c$ -axis, introduction of a point defect or disordering of atomic position in the layer structure by sliding and/or atomic disordering may be plausible. Uniform lattice deformation by grinding has been reported in  $\text{Mg}(\text{OH})_2$  [11]; however expansion of  $c$ -axis, which is perpendicular to the layer structure, was observed in this case.

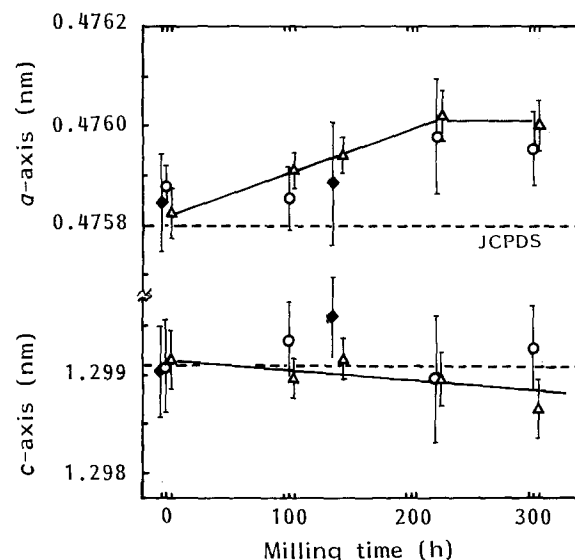


Figure 6 Variation of the lattice constant against milling time. Error bars represent  $\pm 3\sigma$  ( $\sigma$  = standard deviation) range. The dashed lines show reported data for  $\alpha\text{-Al}_2\text{O}_3$  [10].  $\circ$ ,  $S_{0.6}$ ;  $\triangle$ ,  $S_{3.9}$ ;  $\blacklozenge$ ,  $S_{22}$ .

#### 4. Discussion

The relation between applied grinding energy,  $E$ , and particle size,  $R$ , has been examined by many workers. The general formula to represent this relation can be written as follows [12]:

$$dE = kR^{-n}dR \quad (3)$$

where  $k$  is a constant. Rittinger [13], considering the grinding mechanism, suggested that applied energy is almost expended by the increase in surface area of the particles. Assuming that no particle shape change occurs due to the grinding, Equation 3 can be integrated to the following formula:

$$E = k(S - S_0) = k'(1/R - 1/R_0) \quad (4)$$

where  $S$  is surface area;  $S_0$  is initial surface area;  $R_0$  is initial particle size; and  $k$  and  $k'$  are constants. This formula corresponds to an integration of Equation 3 by  $n = 2$ .

On the other hand, Kick [13] proposed a new theory relating applied grinding energy to volume change of particles. The following equation can be derived from this consideration, and corresponds to an integration of Equation 3 by  $n = 1$ .

$$E = k \ln(R_0/R) \quad (5)$$

Bond [14], considering the grinding mechanism, suggested that applied grinding energy is proportional to the variation of particle size, and proposed the intermediate multiplier  $n = 1.5$  for the integration of Equation 3. Thus Equation 6 can be derived.

$$E = k(1/R^{1/2} - 1/R_0^{1/2}) \quad (6)$$

Assuming that the applied grinding energy is proportional to milling time, we attempted to determine the most probable grinding mechanism for three  $\text{Al}_2\text{O}_3$  powders among the above three theories, using Equations 4–6. From the relation between specific surface area and milling time, the data of specimen  $S_{22}$

were found to be best fitted with Equation 4; however the data for the other specimens clearly did not fit with this formula. On the other hand, the data for  $S_{3.9}$  and  $S_{0.6}$  showed a good fit with Equation 5. It was therefore concluded that the grinding mechanism for electrofused  $Al_2O_3$  and low-soda  $Al_2O_3$  was different. This difference was thought to be produced by the difference in physical state of the particles. The particles of electrofused  $Al_2O_3$  were considered to be composed with polygrains, and those of low-soda  $Al_2O_3$  were single-grain, except for agglomerated particles. Therefore breakdown of the particles easily occurred from the grain boundary within a particle in electrofused  $Al_2O_3$ , but not in low-soda  $Al_2O_3$ .

The decrease of particle size in  $S_{3.9}$  and  $S_{0.6}$  was very small even after prolonged grinding. The high Young's modulus and hardness of  $Al_2O_3$  were thought to be likely reasons. The large difference between the sizes of grinding balls and the particles of the specimens may be another reason. Grinding of  $S_{0.6}$  under these conditions, therefore, seemed to reach a grinding limit [15], judging from the data for specific surface area change in this specimen.

The major mechanochemical energy on the particles appeared as variation in crystallite size, lattice deformation, effective temperature factor, and lattice strain. Here the crystallite size corresponds with domain size of the single-crystal region. The lattice deformation means a small expansion and/or shrinkage of the unit cell. Impurities, point defects and distortion of structure were considered for these reasons. The effective temperature factor represents the degree of vibration of atomic position and corresponds to randomization of a structure. The ultimate state is, therefore, an amorphous structure. The lattice strain corresponds to the distribution of compressively and tensilely distorted lattices, and the average lattice size was unchanged in this case. It often originated from the evolution of dislocations.

Fig. 7 shows the relation between crystallite size and lattice strain for each specimen. In the initial grinding stage, mechanochemical energy was solely expended by the decrease in crystallite size of the specimens. After decreasing crystallite size, the lattice strain began to increase. Since the crystallite size of  $S_{0.6}$  was very small from the starting state, the lattice strain increased from the initial stage in this specimen. This crystallite size of 75 nm was considered to be the minimum under these grinding conditions. The lattice strain of  $S_{22}$  was larger than that of  $S_{3.9}$  when comparing these for the same crystallite size. The higher temperature process applied to the former specimen probably causes this difference. Fig. 8 shows the relation between crystallite size and effective temperature factor for each specimen, and shows a similar trend to Fig. 7. The difference in effective temperature factor of  $S_{22}$  and that of  $S_{3.9}$  was clearer than that in lattice strain shown in Fig. 7. This effect was again attributed to the higher temperature process for this specimen. The effective temperature factor of  $S_{22}$  became a closely similar value with that of  $S_{0.6}$  after prolonged grinding, and seemed to be almost saturated by 300 h milling.

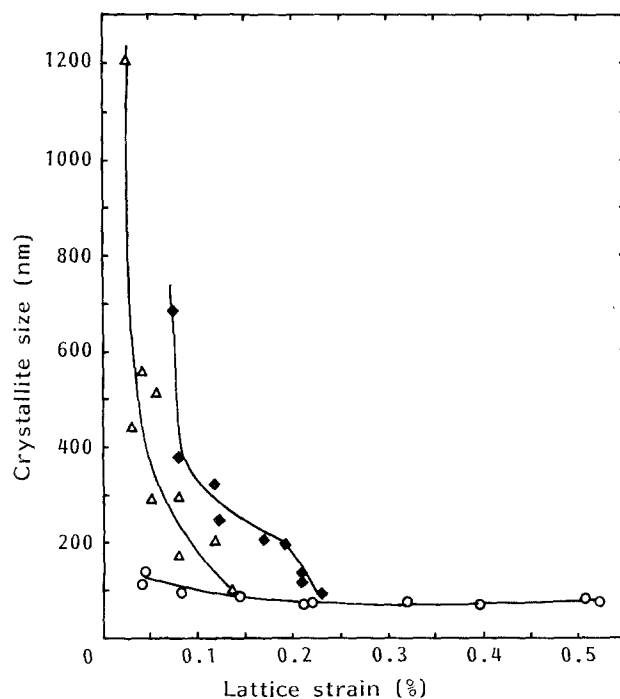


Figure 7 Relation between crystallite size and lattice strain for each specimen.  $\circ$ ,  $S_{0.6}$ ;  $\Delta$ ,  $S_{3.9}$ ;  $\blacklozenge$ ,  $S_{22}$ .

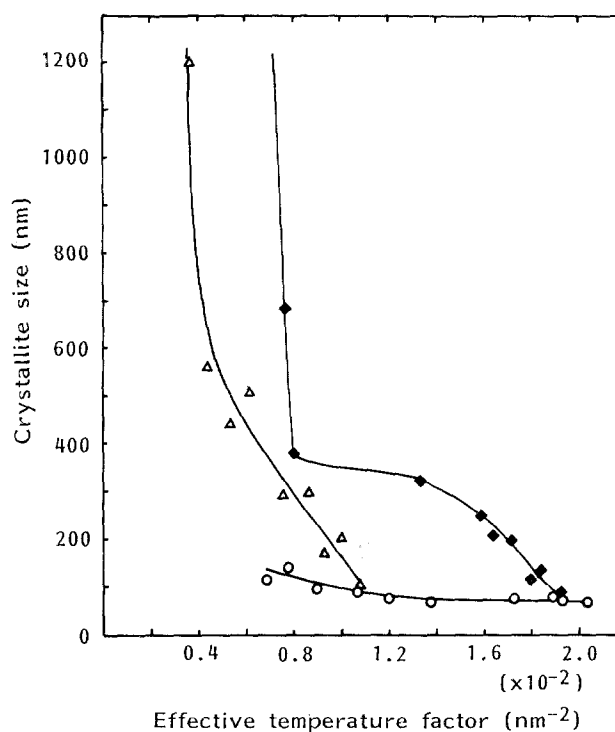


Figure 8 Relation between crystallite size and effective temperature factor for each specimen.  $\circ$ ,  $S_{0.6}$ ;  $\Delta$ ,  $S_{3.9}$ ;  $\blacklozenge$ ,  $S_{22}$ .

Fig. 9 shows the relation between lattice strain and effective temperature factor for each specimen. These data can be represented by three divided straight lines. An interesting point was that the data for  $S_{3.9}$  and  $S_{0.6}$  were plotted on the same straight lines. Initially, the increase in effective temperature factor was much more dominant than that for the lattice strain. Both effective temperature factor and lattice strain increased during the next stage. Finally, the effective temperature factor became saturated but the lattice

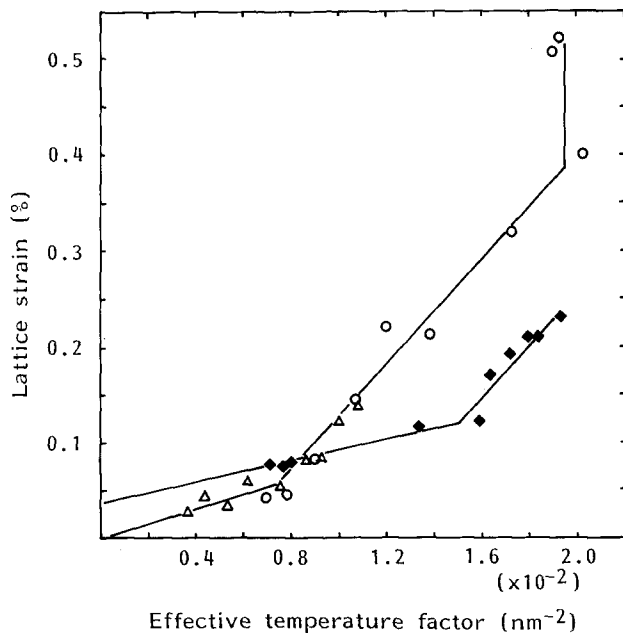


Figure 9 Relation between lattice strain and effective temperature factor for each specimen.  $\circ$ ,  $S_{0.6}$ ;  $\triangle$ ,  $S_{3.9}$ ;  $\blacklozenge$ ,  $S_{2.2}$ .

strain still increased. The data for  $S_{2.2}$  showed a similar trend to low-soda  $Al_2O_3$ , but the data were plotted on different lines. Some difference was observed between the two types of  $Al_2O_3$  specimens, i.e. low-soda and electrofused  $Al_2O_3$ . One difference was that the increase in effective temperature factor of electrofused  $Al_2O_3$  during the initial stage was more noticeable than that in low-soda  $Al_2O_3$ . This means that vibration of atomic position occurred more easily in the electrofused  $Al_2O_3$  than in the low-soda  $Al_2O_3$ . A second point is that a residue lattice strain of around 0.04% was observed in the electrofused  $Al_2O_3$  when the data were extrapolated to  $B_{\text{eff}} = 0$ , while no residue lattice strain was observed in the low-soda  $Al_2O_3$ . It was considered from this result that annealing for the electrofused  $Al_2O_3$  was insufficient under these conditions (e.g. 800°C for 2 h) although for low-soda  $Al_2O_3$  the same annealing conditions were sufficient.

Inagaki *et al.* [2] examined the relations between effective temperature factor and lattice strain for the various materials, and found that the effective temperature factor of most of the materials became saturated by prolonged grinding, but the lattice strain continued to increase. The effective temperature factor was considered to represent the degree of rigidity of the structure. Inagaki *et al.* [2] reported the minimum value for perovskite structure and the maximum value for graphite. Comparing the results for  $Al_2O_3$ , this was ranked in the middle class among the various materials, and had a similar value to  $TiO_2$ .

The mechanochemical effect for these specimens can be summarized as follows:

- 1st stage: decrease in crystallite size;
- 2nd stage: increase in effective temperature factor;
- 3rd stage: increase in both effective temperature factor and lattice strain;

4th stage: saturation of uniform lattice deformation and effective temperature factor, but increase in lattice strain.

This order of mechanochemical factors was considered to reflect the order of susceptibility of deformation. Variation in these factors therefore saturated in the same order. Flexible structures such as graphite [2], molecular bonded layer structures, and  $SiO_2$  [16], constructed by the framework of corner-shared  $SiO_4$  tetrahedra, easily convert to amorphous structures by prolonged grinding and their effective temperature factors can become very large. On the other hand, it was soon saturated in a rigid structure and the mechanochemical energy was stored by the lattice strain instead of the effective temperature factor. It was therefore considered that  $Al_2O_3$  follows the latter case. After 300 h milling, the ground state of three  $Al_2O_3$  specimens reached the following stages: 2nd stage in  $S_{3.9}$ ; 3rd stage in  $S_{2.2}$ ; and 4th stage in  $S_{0.6}$ . These differences were derived from the difference in the physical state of the particles, i.e. polygrain or single grain, and also the particle size of the specimens.

## 5. Conclusions

Three kinds of  $Al_2O_3$  powders, i.e. two kinds of low-soda  $Al_2O_3$  with average particle sizes of 3.9 and 0.6  $\mu\text{m}$  and an electrofused  $Al_2O_3$  with 21.8  $\mu\text{m}$ , were ground by a dry vibration ball mill. The effect of grinding mechanism and the mechanochemical effects on the powders were investigated. To summarize, the following conclusions can be drawn.

1. The grinding mechanisms for  $Al_2O_3$  powders differed with their preparation methods. Variation of particle size,  $R$ , with applied grinding energy was proportional to  $\ln R$  in the low-soda  $Al_2O_3$  and to  $1/R$  in the electrofused  $Al_2O_3$ .
2. The mechanochemical effects on the powders occurred in the order: decrease in crystallite size  $\rightarrow$  increase in effective temperature factor  $\rightarrow$  increase in lattice strain.
3. The increase in the effective temperature factor of electrofused  $Al_2O_3$  occurred much more easily than for low-soda  $Al_2O_3$ .
4. The effective temperature factor reached a constant value of around  $2 \times 10^{-2} \text{ nm}^{-2}$ , and was in the middle class among various inorganic materials.
5. Uniform lattice distortion such as lengthening of the  $a$ -axis in  $\alpha$ - $Al_2O_3$  was observed with grinding.

## Acknowledgements

We are grateful to Professor M. Daimon of Tokyo Institute of Technology for the use of a BET instrument. Part of this work is supported by Nippon Sheet Glass Foundation for Materials Science.

## References

1. K. YAMADA, *Ceramics (Jpn)* **17** (1982) 810.
2. M. INAGAKI, H. FURUHASHI, T. OZEKI and S. NAKA, *J. Mater. Sci.* **8** (1973) 312.

3. T. IWAMOTO and M. SENNA, *J. Soc. Powder Tech. Jpn* **21** (1984) 774.
4. Y. KANNO, *Yogyo Kyokai Shi* **94** (1986) 1218.
5. C. BRODHAG, R. A. L. DREW and L. ZARNON, In "High-Tech Ceramics", Materials Science Monograph 38B edited by P. Vincenzini (Elsevier Amsterdam, 1987) p. 829.
6. M. YASUOKA, K. OKADA, T. HAYASHI and N. OTSUKA, *Ceram. Intern.* (to be published).
7. M. YASUOKA, T. HAYASHI, K. OKADA and N. OTSUKA, *J. Ceram. Soc. Jpn* **98** (1990) 269.
8. W. H. HALL, *Proc. Phys. Soc.* **A62** (1949) 741.
9. T. SAKURAI, RSLC-3(UNICS) Universal Crystallographic Computation Program System (Crystallographic Society of Japan, 1967).
10. JCPDS card No. 10-173.
11. Y. ARAI, T. YASUE and H. MIYAKE, *Nippon Kagaku Kaishi* (1972) 547.
12. W. H. WAKER, W. K. LEWIS, W. H. McADAM and E. R. GILLILAND, "Principles of Chemical Engineering" (McGraw-Hill, 1937) p.
13. K. KUBO, "Mechanochemistry of Inorganic Materials" (Sogo Gijutsu, Tokyo, 1987) p. 99.
14. F. C. BOND, *Trans. AIME Min. Engng* **193** (1952) 484.
15. T. TANAKA, *Kagaku Kogaku* **18** (1954) 160.
16. P. A. REHBINDER and G. S. CHODAKOW, *Silikattechnik* **13** (1962) 200.

*Received 12 September 1990  
and accepted 28 February 1991*